BIOCHEMISTRY
including biophysical chemistry & molecular biology
Article

Biochemistry **2010,** *49,* 9739–9745 9739
DOI: 10.1021/bi1011207

Extensive Small-Angle X-ray Scattering Studies of Blood Coagulation Factor VIIa Reveal Interdomain Flexibility†

Charlotte Rode Mosbæk,*,‡ David Nolan,§ Egon Persson,§ Dmitri I. Svergun,∥ Jens Thostrup Bukrinsky,§ and Bente Vestergaard‡

‡*Department of Medicinal Chemistry, Faculty of Pharmaceutical Sciences, University of Copenhagen, Universitetsparken 2, DK-2100 Copenhagen, Denmark,* §*Novo Nordisk A/S, Novo Nordisk Park, DK-2760 Måløv, Denmark, and* ∥*European Molecular Biology Laboratory, Hamburg Outstation, Notkestrasse 85, D-22603 Hamburg, Germany*

Received July 14, 2010; Revised Manuscript Received September 25, 2010

ABSTRACT: Blood coagulation factor VIIa (FVIIa) is used in the treatment of replacement therapy resistant hemophilia patients, and FVIIa is normally activated upon complex formation with tissue factor (TF), potentially in context with structural rearrangements. The solution behavior of uncomplexed FVIIa is important for understanding the mechanism of activation and for the stability and activity of the pharmaceutical product. However, crystal structures of FVIIa in complex with TF and of truncated free FVIIa reveal different overall conformations while previous small-angle scattering studies suggest FVIIa always to be fully extended in solution. Here, small-angle X-ray scattering analysis of multiple forms of FVIIa and TF under several experimental conditions elaborate extensively on the understanding of the solution behavior of FVIIa. We reveal significant FVIIa domain flexibility in solution, whereas TF has a well-defined conformation. Unspecific formation of dimers of FVIIa is also observed and varies with experimental conditions. In particular, active site-inhibited FVIIa displays a distinct solution behavior different from that of uninhibited FVIIa, which may reflect structural rearrangements causing resistance to activation, thereby emphasizing the connection between the distribution of different conformations of FVII and the mechanism of activation.

Blood coagulation factor VIIa (FVIIa)[1] becomes biologically active after forming a high-affinity complex with the membrane protein tissue factor (TF) (*1*) and catalyzes the activation of coagulation factors IX and X. Recombinant FVIIa is produced as a pharmaceutical product and used in the treatment of hemophilia patients resistant to replacement therapy but can be considered for use in other bleeding situations where it bypasses or helps the regular coagulation cascade. The therapeutic effect is assumed to be largely TF-independent and occurs on the activated platelet surface, whereas in normal physiology the final activation of FVIIa happens by formation of the FVIIa:TF complex. All details of this mechanism of activation are not yet understood.

Zymogen FVII (and FVIIa) is a four-domain protein composed of (*2*) a calcium-binding domain rich in γ-carboxyglutamic acid (Gla, residues 1−44), two epidermal growth factor- (EGF-) like domains (EGF1 and EGF2, residues 45−84 and 85−152), and a serine protease domain (SP, residues 153−406). All four domains interact with TF (*3*).

Posttranslational modifications include N-glycosylations (Asn145, Asn322 (~2.5 kDa each)), O-glycosylations (Ser52, Ser60) (*2*, *4*, *5*), and ten γ-carboxyglutamic acids coordinating seven calcium ions, and finally the EGF1 and SP domains bind two calcium ions (*3*). The total molecular mass (MM) of FVII including posttranslational modifications is 50 kDa.

Since binding of TF is a prerequisite for activation of FVIIa *in vivo*, a structural rearrangement of FVIIa during complex formation may be expected. The mechanism of protein:protein recognition and activation is not fully understood; hence an understanding of the structural aspects of both the free components and the complex is important. However, only structures of active site inhibited FVIIa (ASIS) in complex with TF (ASIS:TF) and of Gla-domainless ASIS (GD-ASIS) have been determined by X-ray crystallography (*3*, *6*, *7*), all revealing different conformations of distal domains.

Small-angle X-ray scattering (SAXS) enables structural analysis of the enzyme in physiologically and drug formulation relevant solutions. Previous SAXS and neutron scattering (SANS) studies concluded that free FVIIa is extended in solution with the N-linked glycans in a nonextended conformation (*8*, *9*). Hence, existing reports in the literature are conflicting and do not reveal the connection between the solution structure of free FVIIa/ASIS and the mode of activation.

Here, we elaborate extensively on the understanding of the solution behavior of FVIIa. In-depth SAXS analysis reveals great conformational freedom of FVIIa domains before complex formation, while TF is conformationally well-defined in solution. Also, we show that the conformational distributions of ASIS and FVIIa are different in solution, which further emphasizes the importance of the conformational freedom of uncomplexed FVIIa.

†This work was financially supported by the Drug Research Academy, DANSCATT, and The Danish Council for Independent Research| Medical Sciences.

*To whom correspondence should be addressed. Telephone: 0045 35336406. Fax: 0045 35336041. E-mail: chrp@farma.ku.dk.

[1]Abbreviations: FVIIa, coagulation factor VIIa; TF, tissue factor; Gla, γ-carboxyglutamic acid rich domain; EGF, epidermal growth factor; SP, serine protease; MM, molar mass; GD, Gla domainless; SAXS, small-angle X-ray scattering; SANS, small-angle neutron scattering; R_g, radius of gyration; BSA, bovine serum albumin; $P(r)$, pair distance distribution functions; D_{max}, maximal dimension; EOM, ensemble optimization method; ASIS, active site-inhibited factor VIIa.

Published on Web 09/28/2010

Table 1: Basic Biophysical Parameters Derived from the Scattering Data and Sample Abbreviations[a]

protein	buffer	pH	MM (kDa)	MM theory (kDa)	R_g primus (nm)	D_{max} (nm)	abbreviation	protein concentration (mg/mL)
FVIIa	10 mM MES	6.0	50	50	3.4	12	$FVIIa_{MES6}$	3.2, 4.7
ASIS	10 mM MES	6.0	59	50	3.3	12	$ASIS_{MES6}$	3.4, 5.2
	10 mM MES	7.4	60	50	3.2	12.5	$ASIS_{MES7.4}$	2.8, 4.9
	10 mM HIS	6.0	58	50	3.4	14	$ASIS_{HIS6}$	3.0, 4.7
	10 mM HEPES	7.4	58	50	3.3	13	$ASIS_{HEPES7.4}$	1.8, 2.7, 3.7
	10 mM MES, 40 mM $CaCl_2$	6.0	58	50	3.2	12	$ASIS_{Ca}$	1.7, 3.2
GD-ASIS	10 mM MES	6.0	46	40	2.7	14	$GDASIS_{MES6}$	1.7, 3.5, 7
GD-FVIIa	10 mM MES	6.0	56	40	2.8	10	$GDFVIIa_{MES6}$	2.9, 4.1, 6.2
ASIS:TF	10 mM MES	6.0	72	74	3.5	13	$ASIS:TF_{MES6}$	2.0, 2.7, 3.9
	10 mM HEPES	7.4	72	74	3.4	12.5	$ASIS:TF_{HEPES7.4}$	2.1, 2.9, 4.1
TF	10 mM MES	6.0	22	24	2.5	9.5	TF_{MES6}	2.0, 4.1, 6.2
TF	10 mM HEPES	7.4	22	24	2.5	10	$TF_{HEPES7.4}$	1.8, 3.9
BSA	50 mM HEPES	7.4		66	3	9		6.6

[a]The MM and R_g are calculated from the forward scattering, while D_{max} is derived from the pair distance distribution function. The protein concentrations indicate the individual samples measured. Each concentration was measured twice.

EXPERIMENTAL PROCEDURES

Preparation of Protein Samples. FVIIa was produced and purified as described previously (*2*, *10*). All subsequent purifications of individual forms were done using an anion-exchange Q-Sepharose FF column. Active site-inhibited FVIIa (ASIS) was prepared using H-D-Phe-Phe-Arg-chloromethyl ketone and purified as above. Gla-domainless (GD) proteins were obtained using 0.2% cathepsin G in 20 mM Tris, 2 mM EDTA, and 50 mM NaCl, pH 9.0, and purified from intact protein by applying a gradient of 0−0.4 M NaCl. A complex between ASIS and recombinant soluble TF (provided by Novo Nordisk A/S) was prepared using TF in 15% molar excess.

All samples contain 100 mM NaCl, 2 mM $CaCl_2$, and 2 mM DTT buffered with 10 mM MES, histidine, or HEPES buffer at pH 6.0 or 7.4 (Table 1). Additional samples containing 40 mM $CaCl_2$ were prepared immediately prior to SAXS measurements. All other samples were dialyzed 24 h against the respective buffers and concentrated using Amicon Ultra centrifugal filters (MMCO 10 kDa). The purity of all samples was tested using SDS−PAGE and dynamic light scattering (see Supporting Information Table S1 and Figure S1).

Small-Angle X-ray Scattering Data Collection and Initial Evaluation. SAXS data were collected (1.8−6.6 mg/mL) using synchrotron radiation following standard procedures at beamline X33 at the European Molecular Biology Laboratory on the DORIS III storage ring (DESY, Hamburg, Germany). A momentum transfer range of 0.08−5.0 nm^{-1} ($s = 4\pi \sin(\theta)/\lambda$, 2θ is the scattering angle, λ is the wavelength (λ = 1.5 Å)) was covered using exposure times of 2 min, 8 °C. The detector response corrected data were normalized to the intensity of the incident beam. Repeated exposures resulted in no observable X-ray-induced damage. Data analysis was performed using the software suite ATSAS (*11*, *12*). Data from several protein concentrations (Table 1) without concentration effects were merged to give the final data file. The radius of gyration (R_g) was evaluated by the Guinier approximation, and the average molecular mass (MM) was estimated from the extrapolated forward scattering intensity $I(0)$ using a reference solution of bovine serum albumin (BSA). The pair distance distribution functions ($P(r)$) were evaluated using GNOM (*13*, *14*), yielding also the maximal dimension (D_{max}) within the scatterer.

Ab Initio Modeling. *Ab initio* structures were obtained using the program DAMMIF (*15*). A simulated annealing protocol was used to build a compact bead model of uniform scattering length density, while minimizing the discrepancy between the experimental and calculated curves at low resolution (scattering angles up to 2.8 nm^{-1} were used). Ten individual models were averaged using the program DAMAVER (*16*). A filtering procedure resulted in a final averaged model which was used as the starting volume for the calculation of ten refined individual models which were averaged and filtered with an excluded volume in accordance with individual models.

Creation of Theoretical Models. All handling of PDB files was done using PyMOL(*17*). Three PDB files of ASIS showing different positions of the EGF1 domain were selected (1DAN (ASIS:TF), 1QFK, and 1DVA (GD-ASIS)) and defined as positions 1, 2, and 3, respectively. Water atoms were removed. The first two residues of a missing loop (Lys143−Arg152) were added by superpositioning of PDB files 1KLJ, 1KLI (EGF2-SP), and 1QFK (GD-FVIIa) on 1DAN, and the remainder of the loop was built by hand. Only short N-glycans are visible in the crystal structures. The Gla domain from 1DAN was added to 1DVA and 1QFK by superpositioning of the EGF1 domain. Missing loops in TF were added to 1DAN from the coordinates of 1Z6J (ASIS:TF).

Models were created in PyMOL by rotating individual domains as rigid bodies (Figure 1A). Because of multiple interactions between the EGF2 and SP domains, they were regarded as a single body. The EGF1 domain was positioned by rotation around residue 85 in the EGF2 linker equally covering the conformational space while avoiding clashes. Because of software demands, alanine-based models corresponding to three different types of N-glycans (compact, bent, and stretched; see Figure 1A) were built using alanine residues corresponding to the molecular mass of the N-glycans; hence this results in scattering as expected from the glycans.

The glycosylation models were rotated from the glycosylation sites, resulting in a pool of 8167 theoretical models of GD-ASIS with EGF1 and glycans in different positions. A total of 145 models were selected, and the Gla domain was attached and rotated around the linker, resulting in a pool of 1010 structures of the full-length protein. The complex between FVIIa and TF is regarded as a rigid body except for the carbohydrates. A pool of 780 complex structures was created.

Dimers of ASIS, GD-ASIS, and the ASIS:TF complex were created using FTDock (*18*). A pool of 10000 dimers was created from one conformation (position 1, without glycosylations) of each and evaluated in the FTDock software for plausibility.

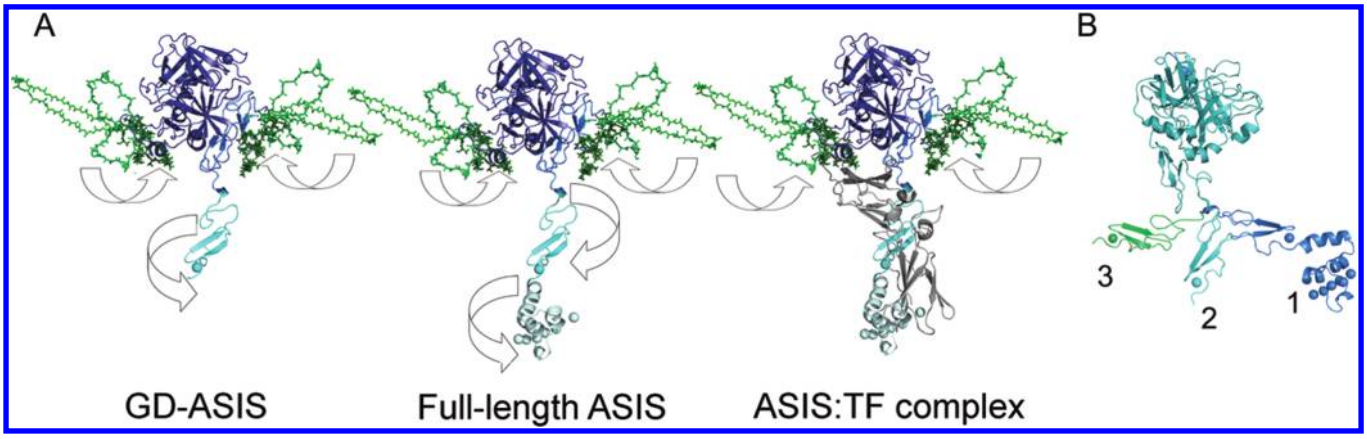

FIGURE 1: (A) Generation of theoretical monomers. Domains are shown in blue colors, modeled glycans by shades of green, and TF is shown in gray. Arrows illustrate the rotation of individual domains. (B) X-ray crystal structures of FVIIa (PDB codes 1DAN (ASIS:TF), 1QFK, 1DVA (GD-ASIS)), superimposed on the SP domain, revealing different orientations of the EGF1 domain. Calcium ions are shown as spheres.

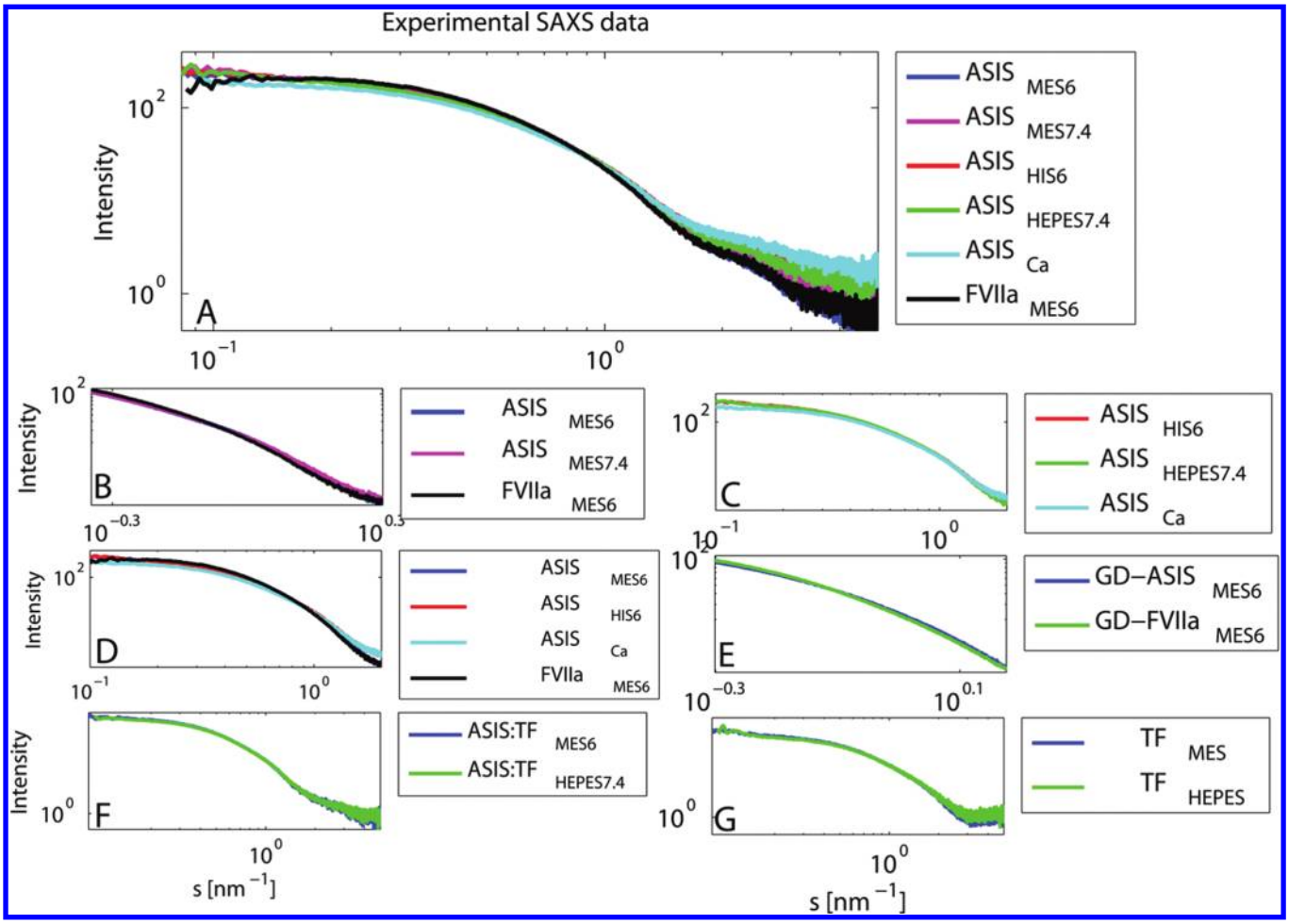

FIGURE 2: (A) Scattering curves of ASIS and FVIIa. (B−D) Zooms of (A). (E) Scattering curves with zoom of GD-ASIS and GD-FVIIa. (F) Scattering curves of the ASIS:TF complex. (G) Scattering curves of TF. All curves are scaled in the area 0.7−0.9 nm^{-1}.

The final dimer pools consisted of the 1000 highest scoring structures af ASIS and GD-ASIS, respectively, and 600 structures representing ASIS:TF complex dimers.

All pools of structures were created based on ASIS structures. These pools were also applied when analyzing data from uninhibited FVII, since the differences between high-resolution structures of ASIS and FVII are beyond the resolution of the current analysis.

Ensemble Optimization Method (EOM). Theoretical scattering curves were calculated using CRYSOL (*19*) with default parameters. Ensembles of 20 structures were calculated using Gajoe from the EOM package (*20*) to obtain the best fit between experimental scattering and the calculated scattering from a mixture of structures, applying 5000 generations with default parameters. Fits were calculated from pools with and without dimers.

RESULTS

Basic Observations from SAXS Data. Table 1 presents a list of collected SAXS data and abbreviations. The observed average

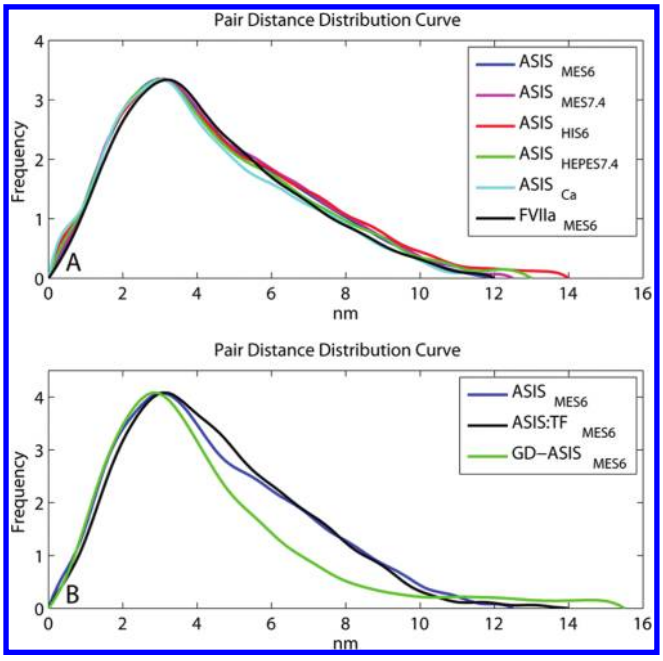

FIGURE 3: $P(r)$ for (A) ASIS and FVIIa under different experimental conditions and (B) ASIS, ASIS:TF, and GD-ASIS under similar experimental conditions. All curves are normalized at $d = 3$ nm.

MM of ASIS in selected buffers was 58−60 kDa. Assuming that only monomers and dimers were present, this corresponds to 16−20% dimer. The R_g values of ASIS and FVIIa samples correspond to the theoretical calculated values from a fully extended conformation (Supporting Information Table S2). However, the experimental D_{max} values significantly exceed those of the monomer which together with the observed increased MM points to the presence of dimers. Since the calculated R_g is an average for all scatterers, the average R_g of monomers would be smaller than that of an extended conformation.

Directly observable changes are evident in scattering from (hence the solution structure of) ASIS in different buffers (Figure 2). $ASIS_{MES6}$ and $ASIS_{MES7.4}$ are similar and so are $ASIS_{HIS6}$ and $ASIS_{HEPES7.4}$, which are again distinct from $ASIS_{Ca}$. Surprisingly, data from uninhibited $FVIIa_{MES6}$ deviate from inhibited $ASIS_{MES6}$. When comparing the $P(r)$ functions (Figure 3), all ASIS samples have a typical reoccurring pair distance around 3 nm. In accordance with the suggested presence of dimers in solution, most $P(r)$ functions display a slowly decaying tail toward D_{max}.

$ASIS{:}TF_{MES6}$ was prepared using 15% excess of TF and has an average MM of 72 kDa, hence containing 15% free TF, 77% complex, and 8% dimer. The complex thus has a lower tendency to form dimers than ASIS. Scattering from $ASIS{:}TF_{HEPES7.4}$ and $ASIS{:}TF_{MES6}$ is identical; i.e., the solution structure is less sensitive to buffer composition than ASIS. Likewise, the scattering curves from TF_{MES6} and $TF_{HEPES7.4}$ are identical.

The scattering curves of $GD\text{-}ASIS_{MES6}$ and $GD\text{-}FVIIa_{MES6}$ deviate at lower scattering angles, hence displaying different solution behaviors at identical experimental conditions.

The *ab initio* model of TF (Figure 4) corresponds well to the X-ray crystal structure of TF from the ASIS:TF complex. Attempts to generate *ab initio* models of FVIIa and the complex (Supporting Information Figure S5) confirm the suggested partial formation of dimers (*21*).

Basic Observations from X-ray Crystal Structures and Previous Scattering Data. The experimental solution parameters have been compared to calculated values (Supporting

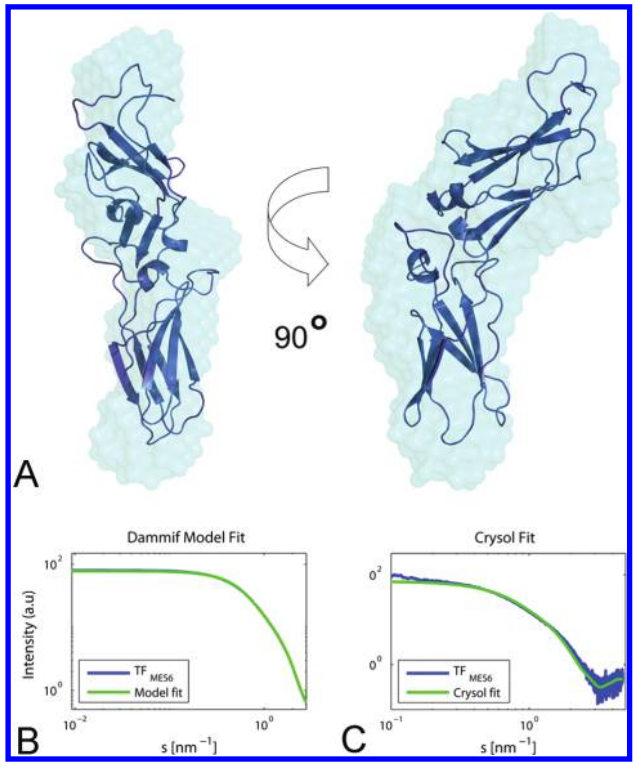

FIGURE 4: (A) *Ab initio* model of TF_{MES6} (light blue) superimposed on the X-ray crystal structure of TF (dark blue, extracted from PDB code 1DAN), (B) fit to the experimental data, and (C) fit to the X-ray crystal structure of TF in complex with ASIS (PDB entry 1DAN).

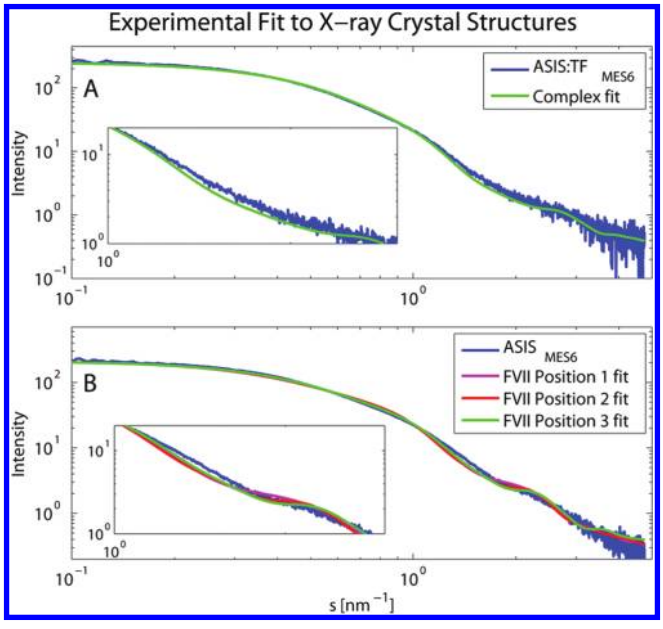

FIGURE 5: Comparison of (A) $ASIS{:}TF_{MES6}$ and (B) $ASIS_{MES6}$ to theoretical calculated scattering curves of X-ray crystal structures of ASIS:TF and ASIS, respectively, with modeled glycosylations.

Information Table S2) based on high-resolution structures (with the EGF1 (and Gla) domain in different positions, Figure 1B) and with the values previously reported from a SAXS/SANS study (*8*, *9*). Three types of glycans (compact, bent, stretched) were modeled before comparison.

The theoretical R_g is strongly influenced by the conformation of the modeled glycans. Thus it is possible to obtain the same R_g with concurrent different positions of glycans and the Gla domain. R_g and D_{max} from previously reported scattering studies (*8*)

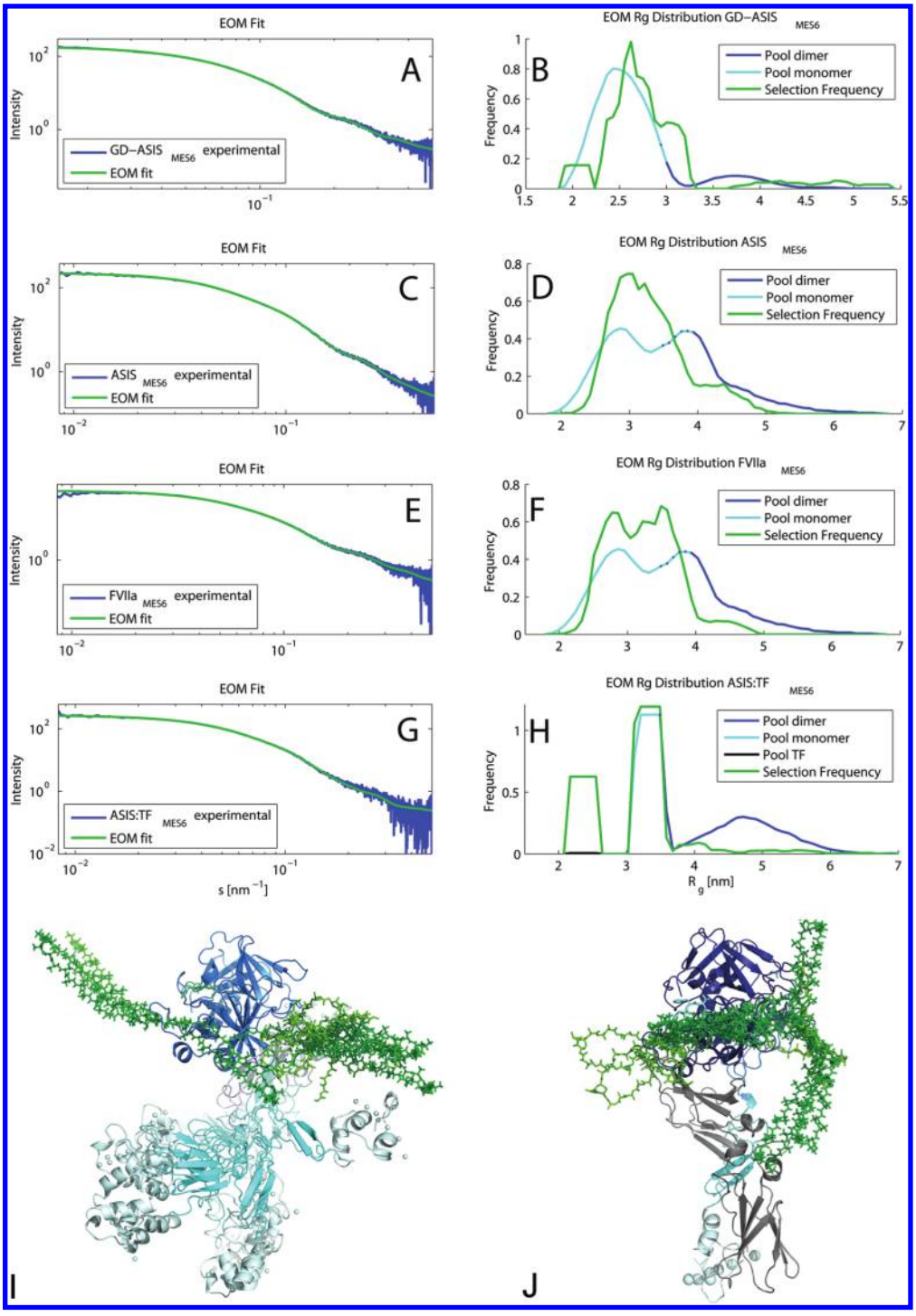

FIGURE 6: EOM fit (A, C, E, G) to the experimental scattering curve and R_g distributions (B, D, F, H) corresponding to the pool of structures (dimers are in blue, monomers are in cyan, and TF is in black) and the 50 best selected ensembles (in green) of GD-ASIS (A, B), ASIS (C,D), FVIIa (E,F), and ASIS:TF (G, H) and selected conformations of the domains and glycosylations are shown for (I) ASIS and (J) ASIS:TF.

would be in accordance with several plausible theoretical conformations and not only the suggested conformation. It is evident that none of the crystal structures describe the solution structure of FVIIa/ASIS and ASIS:TF (15% free TF is not accounted for; see Supporting Information for an oligomer analysis including free TF) (Figure 5); in particular a deviation is seen at scattering angles between 0.1 and 2.5 nm^{-1}.

Analysis of Ensembles in Solution. Primary analysis of SAXS data and initial modeling attempts indicate that the samples are heterogeneous. We expect this to be in part due to formation of dimers and in part due to significant structural flexibility. Flexible systems can with advantage be analyzed using methods which take into account solution behavior as well as high-resolution details (*22*). Therefore, we applied EOM (*20*), which selects ensembles of theoretical scattering curves from large pools of structures in accordance with experimental data.

Initially, the data from GD proteins were analyzed. This structure is expected to have the lowest degree of flexibility; hence the data are easier to interpret, and the results may be extrapolated to other samples. GD-ASIS$_{MES6}$ was analyzed using a pool of 8167 monomers and 1000 dimers with flexible glycans, and a good fit (Figure 6 and Table 2) was obtained. It was not possible to obtain

Table 2: EOM Parameters for 20 Structures Selected by EOM from a Pool of Monomers and Dimers[a]

protein	selected monomers	selected dimers	average R_g (nm)	Chi	dimer content % (mol)
$ASIS_{MES6}$	16−17	3−4	3.4	1.45	15−20
$ASIS_{MES7.4}$	16−17	3−4	3.4	1.41	15−20
$ASIS_{HIS6}$	16−18	2−4	3.7	1.59	10−20
$ASIS_{HEPES7.4}$	17−18	2−3	3.6	1.58	10−15
$ASIS_{Ca}$	19−20	0−1	3.4	1.4	0−5
$FVIIa_{MES6}$	15−16	4−5	3.3	1.7	20−25
$GDASIS_{MES6}$	18−19	1−2	3	2.13	5−10
$ASIS:TF_{MES6}$	11	1−2 TF:5−7	3.3	1.7	15
$ASIS:TF_{HEPES7.4}$	12−14	1 TF:5−7	3.2	1.67	7

[a]The average R_g and the selected monomers, dimers, and TF are the results of 50 ensembles of each 20 structures, while the Chi value represents the best fitting ensemble.

any adequate fit with a pool consisting of monomers only or a pool of monomers and dimers with stationary glycans (see Supporting Information). In conclusion, both glycans and the EGF1 domain are flexible in GD-ASIS, and 5−10% dimers exist in solution. The selected pool of dimers does not describe specific dimers; rather the collected distribution of overall size and conformation corresponds to the actual dimer pool.

A total of 1010 possible ASIS monomer structures and 1000 dimer structures were analyzed against ASIS and FVIIa data. Very good fits were obtained (Figure 6, Supporting Information Figures S2 and S3), and the calculated percentage of selected dimers agrees (Table 2) with the calculated average MM. A broad distribution of R_g values is observed for all samples, indicating flexibility within the protein under all investigated buffer compositions.

Data from $ASIS_{MES6}$ and $ASIS_{MES7.4}$ reveal comparable R_g distributions (2.1−5.3 nm, Figure 6 and Supporting Information Figure S2), covering a broad R_g range and including dimers. For $ASIS_{HIS6}$ and $ASIS_{HEPES7.4}$ the distribution of R_g values is broader, including dimers with an R_g up to 6.7 nm. $ASIS_{Ca}$ was the only sample that could be fitted with a selection of monomers only, but also here a highly flexible pool of structures is suggested. As a complementary approach, rigid body modeling was attempted, not resulting in adequate fits from a single monomeric structure (see Supporting Information for details).

The ASIS:TF complex was studied using 780 ASIS:TF monomers (with flexible glycans) and 600 dimers. A good fit to $ASIS:TF_{MES6}$ was obtained only when scattering curves representing free TF were present, in accordance with the excess of TF in the sample preparation. Even in the presence of TF, adequate fits were not obtained without accounting for dimers (see Supporting Information). No domain flexibility was needed to describe the ASIS:TF complex supporting the formation of a rigid entity.

DISCUSSION

A structural understanding of the free FVIIa and TF components is important for addressing the mechanism of activation. However, there is a lack of consensus in the literature regarding the structure of free FVIIa in solution. Crystal structures have revealed several orientations of the EGF1 domain and no extensive contacts between the EGF1, EGF2, and Gla domains. This suggests that free FVIIa in solution could have an overall flexible conformation and is supported by normal-mode analysis which indicates large fluctuations (*23*). In addition, glycans are known to be flexible in solution. In contrast to the expected flexibility, previous SAXS/SANS studies indicate that glycans are compact and that the overall structure of ASIS is fully elongated in solution (*8*, *9*).

In this study, we analyze multiple versions of factors in solution, including truncated versions. The multitude of data enables an in-depth analysis of the solution behavior of the protein. We show that there is significant flexibility at hinge points between the Gla and EGF1/EGF2 domains within ASIS/FVIIa and further (in contrast to previous reports) that the glycans are flexible and extend from the protein surface. While glycan flexibility classically ascribes to solubility enhancement and reduction of aggregation, the overall conformational flexibility of individual domains may facilitate the search for and binding of FVIIa to TF and contribute to the necessity of the rigid FVIIa:TF complex formation for *in vivo* activity of FVIIa. We see a general tendency of 9−15% formation of dimers for ASIS/FVIIa and the ASIS:TF complex. The EOM anlaysis reveals a broad distribution of dimer conformations which indicates that the dimers are unspecific. An analysis of low scattering angles in the raw data files further shows that the increased molecular mass and tendency of $P(r)$ functions with long decaying tails could indeed be interpreted as dimers and not general aggregation. We also observe a variation of the solution behavior between different experimental conditions and detect a distinctly different scattering pattern and a difference in the distribution of conformations and the amount of dimer, when calcium is present. This confirms the importance of calcium ions, which is in accordance with X-ray crystal structures showing several calcium ions coordinated to EGF2, SP, and the multiple γ-glutamic acids present in the Gla domain, which may affect the distribution of conformations or induce unexpected interactions when unshielded by calcium. These latter observations suggest that SAXS solution analysis may assist further optimization of formulation conditions for the pharmaceutical product. Also, in the presence of Ca^{2+} at physiological conditions the protein displays great flexibility in solution. Moreover, ASIS and the uninhibited counterpart, FVIIa, display different solution behavior. The change in distribution of conformations in solution coincides with a measurable effect on the affinity for TF (*24*). Comparison of crystal structures of truncated ASIS and FVIIa (*25*) suggests that restricted movement of the flexible N-terminal tail starting with residue 153, or of the so-called 170 loop and its carbohydrate (linked to Asn322) (*26*), plays a role in defining the difference in affinity for TF. However, neither of the two mentioned regions interact with TF, and no further structural changes are observed in the SP domain where the two areas reside. Hence the crystal structures alone do not explain the difference in affinity to TF. Our SAXS solution data from ASIS and FVIIa differ significantly. It is evident that the whole distribution of conformations shifts when the factor is inhibited and changes at ranges larger than the rearrangement of the

N-terminus and 170 loop would be necessary to explain the large observable differences. The shift in the conformational distribution revealed by EOM hence reflects a statistically different solution behavior of the inhibited and uninhibited forms of the protein. We suggest that this shift in conformational distribution influences the affinity toward TF. Further considering that our studies confirm the notion that TF has a rigid structure in solution, it is plausible that the formation of the FVIIa:TF complex is facilitated by the flexibility of FVIIa and that the complex formation reduces the domain movements within FVIIa. Future enhancement of the potency of the pharmaceutical could be influenced by modifications shifting the overall conformational distribution of the uncomplexed protein, an approach which would have some novelty compared to the more static picture of proteins which normally is the basis for optimization of protein pharmaceuticals.

In summary, our results clarify the understanding of the solution behavior of FVIIa and connect the previously observed different crystal structures of FVIIa/ASIS with existing reports on affinity to the activating TF. Our investigations clearly illustrate the necessity of having a large pool of SAXS data to enable firm conclusions regarding flexible proteins. Also, we show the usefulness of structural solution studies for formulation considerations, and we suggest that an expanded consideration of multiple conformations (in contrast to one single static structure) is the correct basis for further improving the potency of FVIIa.

ACKNOWLEDGMENT

We particularly thank Anette Østergaard for being helpful with protein preparations. Proteins were kindly provided by Novo Nordisk A/S.

SUPPORTING INFORMATION AVAILABLE

SDS−PAGE verification, dynamic light scattering data, additional EOM analysis, SASREF rigid body analysis, *ab initio* modeling using DAMMIF and OLIGOMER analysis. This material is available free of charge via the Internet at http://pubs.acs.org.

REFERENCES

1. O'Brien, D. P., Kemball-Cook, G., Hutchinson, A. M., Martin, D. M., Johnson, D. J., Byfield, P. G., Takamiya, O., Tuddenham, E. G., and McVey, J. H. (1994) Surface plasmon resonance studies of the interaction between factor VII and tissue factor. Demonstration of defective tissue factor binding in a variant FVII molecule (FVII-R79Q). *Biochemistry 33*, 14162–14169.
2. Hagen, F. S., Gray, C. L., O'Hara, P., Grant, F. J., Saari, G. C., Woodbury, R. G., Hart, C. E., Insley, M., Kisiel, W., and Kurachi, K. (1986) Characterization of a cDNA coding for human factor VII. *Proc. Natl. Acad. Sci. U.S.A. 83*, 2412–2416.
3. Banner, D. W., D'Arcy, A., Chene, C., Winkler, F. K., Guha, A., Konigsberg, W. H., Nemerson, Y., and Kirchhofer, D. (1996) The crystal structure of the complex of blood coagulation factor VIIa with soluble tissue factor. *Nature 380*, 41–46.
4. Bjoern, S., Foster, D. C., Thim, L., Wiberg, F. C., Christensen, M., Komiyama, Y., Pedersen, A. H., and Kisiel, W. (1991) Human plasma and recombinant factor VII. Characterization of O-glycosylations at serine residues 52 and 60 and effects of site-directed mutagenesis of serine 52 to alanine. *J. Biol. Chem. 266*, 11051–11057.
5. Klausen, N. K., Bayne, S., and Palm, L. (1998) Analysis of the site-specific asparagine-linked glycosylation of recombinant human coagulation factor VIIa by glycosidase digestions, liquid chromatography, and mass spectrometry. *Mol. Biotechnol. 9*, 195–204.
6. Dennis, M. S., Eigenbrot, C., Skelton, N. J., Ultsch, M. H., Santell, L., Dwyer, M. A., O'Connell, M. P., and Lazarus, R. A. (2000) Peptide exosite inhibitors of factor VIIa as anticoagulants. *Nature 404*, 465–470.
7. Pike, A. C., Brzozowski, A. M., Roberts, S. M., Olsen, O. H., and Persson, E. (1999) Structure of human factor VIIa and its implications for the triggering of blood coagulation. *Proc. Natl. Acad. Sci. U.S.A. 96*, 8925–8930.
8. Ashton, A. W., Boehm, M. K., Johnson, D. J., Kemball-Cook, G., and Perkins, S. J. (1998) The solution structure of human coagulation factor VIIa in its complex with tissue factor is similar to free factor VIIa: a study of a heterodimeric receptor-ligand complex by X-ray and neutron scattering and computational modeling. *Biochemistry 37*, 8208–8217.
9. Ashton, A. W., Kemball-Cook, G., Johnson, D. J., Martin, D. M., O'Brien, D. P., Tuddenham, E. G., and Perkins, S. J. (1995) Factor VIIa and the extracellular domains of human tissue factor form a compact complex: a study by X-ray and neutron solution scattering. *FEBS Lett. 374*, 141–146.
10. Thim, L., Bjoern, S., Christensen, M., Nicolaisen, E. M., Lund-Hansen, T., Pedersen, A. H., and Hedner, U. (1988) Amino acid sequence and posttranslational modifications of human factor VIIa from plasma and transfected baby hamster kidney cells. *Biochemistry 27*, 7785–7793.
11. Konarev, P. V., Volkov, V. V., Sokolova, A. V., Koch, M. H. J., and Svergun, D. I. (2003) PRIMUS: a windows PC-based system for small-angle scattering data analysis. *J. Appl. Crystallogr. 36*, 1277–1282.
12. Konarev, P. V., Petoukhov, M. V., Volkov, V. V., and Svergun, D. I. (2006) ATSAS 2.1, a program package for small-angle scattering data analysis. *J. Appl. Crystallogr. 39*, 277–286.
13. Svergun, D. I., Semenyuk, A. V., and Feigin, L. A. (1988) Small-angle-scattering-data treatment by the regularization method. *Acta Crystallogr. A 44*, 244–250.
14. Svergun, D. I. (1992) Determination of the regularization parameter in indirect-transform methods using perceptual criteria. *J. Appl. Crystallogr. 25*, 495–503.
15. Franke, D., and Svergun, D. I. (2009) DAMMIF, a program for rapid ab-initio shape determination in small-angle scattering. *J. Appl. Crystallogr. 42*, 342–346.
16. Volkov, V V., and Svergun, D. I. (2003) Uniqueness of ab initio shape determination in small angle scattering. *J. Appl. Crystallogr. 36*, 860–864.
17. DeLano, W. L. (2008) The PyMOL Molecular Graphics System, DeLano Scientific LLC, Palo Alto, CA, USA.
18. Gabb, H., Jackson, R. M., and Sternberg, M. J. E. (1997) Modelling protein docking using shape complementarity, electrostatics and biochemical information. *J. Mol. Biol. 272*, 106–120.
19. Svergun, D. I., Barberato, C., and Koch, M. H. J. (1995) Crysol - a program to evaluate X-ray solution scattering of biological macromolecules from atomic coordinates. *J. Appl. Crystallogr. 28*, 768–773.
20. Bernadó, P., Mylonas, E., Petoukhov, M. V., Blackledge, M., and Svergun, D. I. (2007) Structural characterization of flexible proteins using small-angle X-ray scattering. *J. Am. Chem. Soc. 129*, 5656–5664.
21. Bernadó, P., Pérez, Y., Svergun, D. I., and Pons, M. (2008) Structural characterization of the active and inactive states of src kinase in solution by small-angle X-ray scattering. *J. Mol. Biol. 376*, 492–505.
22. Rambo, R. P., and Tainer, A. T. (2010) Bridging the solution divide: comprehensive structural analyses of dynamic RNA, DNA, and protein assemblies by small-angle X-ray scattering. *Curr. Opin. Struct. Biol. 20*, 128–137.
23. Soejima, K., Kurihara, Y., Kamiya, K., and Umeyama, H. (1999) Dynamic character of the complex of human blood coagulation factor VIIa with the extracellular domain of human tissue factor: a normal mode analysis. *FEBS Lett. 463*, 19–23.
24. Sørensen, B. B., Persson, E., Freskgard, P.-O., Kjalke, M., Ezban, M., Williams, T., and Rao, L. V. M. (1997) Incorporation of an active site inhibitor in factor VIIa alters the affinity for tissue factor. *J. Biol. Chem. 272*, 11863–11868.
25. Sichler, K., Banner, D. W., Dárcy, A., Hopfner, K.-P., Huber, R., Bode, W., Kresse, G.-B., Koptzki, E., and Brandstetter, H. (2002) Crystal structures of uninhibited factor VIIa link its cofactor and substrate-assisted activation to specific interactions. *J. Mol. Biol. 322*, 591–603.
26. Olsen, O. H., Rand, K. D., Østergaard, H., and Persson, E. (2007) A combined structural dynamics approach identifies a putative switch in factor VIIa employed by tissue factor to initiate blood coagulation. *Protein Sci. 16*, 671–682.